AIAA–2004–1243

Separation Control by Self-Activated Movable Flaps

M. Schatz, T. Knacke and F. Thiele
Hermann-Föttinger-Institute for Fluid Mechanics
Technical University Berlin, Germany

R. Meyer, W. Hage and D.W. Bechert
German Aerospace Center (DLR) Berlin, Germany

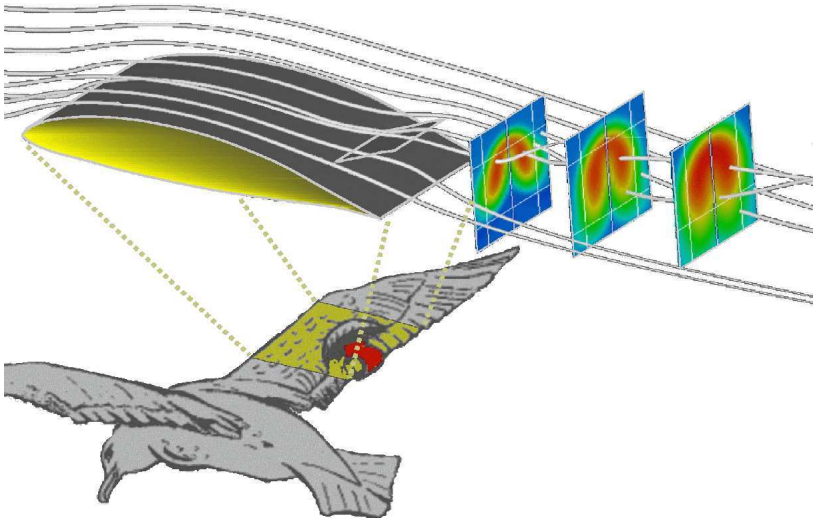

42th AIAA Aerospace Sciences Meeting & Exhibit
5-8 January 2004 / Reno, NV

Separation Control by Self-Activated Movable Flaps

Markus Schatz, Thilo Knacke and Frank Thiele
Technical University of Berlin, Hermann-Föttinger-Institute for Fluid Dynamics
10623 Berlin, Germany
and
Robert Meyer, Wolfram Hage and Dietrich W. Bechert
German Aerospace Center (DLR)
10623 Berlin, Germany

Separation control is also an important issue in the physiology of birdflight. In this paper the adaption of the separation control mechanism by bird feathers to the requirements of engineering applications is described in detail. Self-activated movable flaps similar to artificial bird feathers represent a high-lift system enhancing the maximum lift of airfoils. Their effect on the unsteady flow around a two-dimensional airfoil configuration is investigatd by a joint numerical and experimental study. First, attention is paid to the automatic opening and closing mechanism of the flap. Following this, its beneficial effect on the lift is investigated for varying incidences and flap configurations. In-depth analysis of experimental and numerical results provides a detailed description of the important phenomena and the effect of self-adjusting flaps on the flow around the airfoil. In the second part of this paper, a contribution to verification of the applicability of Unsteady Reynolds-averaged (URANS) approaches using statistical turbulence models for unsteady flows with special respect to the occuring turbulent time-scales is given for which comparison to the results of a hybrid simulation based on URANS and Large-Eddy-Simulation (LES) is made. Finally, flight experiments using an aircraft with movable flaps fitted on its laminar wing are described.

Nomenclature

b	wing span
c	chord length
c_L, c_D	lift- and drag coefficient
c_F	flap-moment coefficient
c_G	gravity-moment coefficient
c_R	reverse flow parameter
k	turbulent kinetic energy
l_F	flap length
L_t	turbulent length scale
M_F	flap moment due to fluid force
M_G	flap moment due to gravity
Re	Reynolds number based on chord length
St	Strouhal number based on flap length
u_0	inflow velocity
x_d	detachment position
α	angle of attack
β, β_{max}	flap deflection angle, maximum angle
ϱ	density
ω	specific turbulent dissipation

Introduction

Birds have a very effective means of dealing with flow separation on their wings. Once the attention has been drawn to it, it is comparatively easy to observe on almost any bird: During the landing approach or in gusty winds, the feathers on the upper surface of bird wings tend to pop up (Fig. 1).

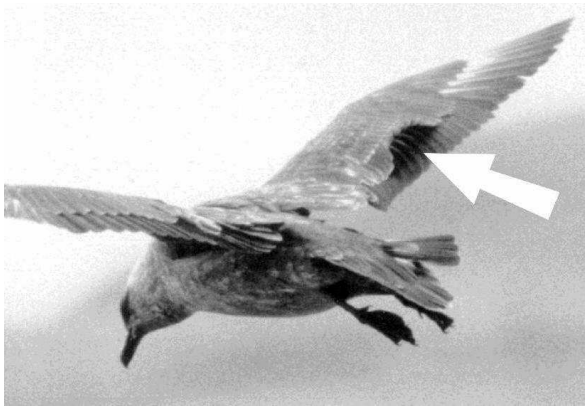

Fig. 1 A bird's wing with popped up feathers to prevent further proliferation of flow separation. (photo by I. Rechenberg).

W. Liebe interpreted this behaviour as a biological high-lift device.[1] It seemed a likely supposition that *flow separation* could be delayed, with *higher lift* allowing *lower flight speeds*. He suggested the adoption of the same principle to engineering application. At the former German Aeronautical Establishment (DVL) flight experiments with a Messerschmitt Me 109 fighter airplane were car-

ried out as early as 1938. A piece of leather was attached to the upper side of one wing. The ensuing aerodynamic asymmetry of the wings caused the aircraft to be difficult to handle, particularly at high angles of attack. The problems occurring in this initial test prevented further investigation of the concept.

Liebe's original idea was that once separation starts to develop on a wing, reversed flow is bound to occur in the separation regime.[1] Under these locally reversed flow conditions, light feathers would pop up, acting like a brake on the spreading of flow separation towards the leading edge. Liebe was aware of the fact that flow separation is often three-dimensional with variable patterns in the spanwise direction. Thus, he considered it essential to be able to interact locally with separation regimes (Fig. 1). Following Liebe's ideas, a few tentative flight experiments have been carried out with small movable plastic sheets installed on a glider wing on the upper surface near the trailing edge. A slightly augmented behaviour of that glider aircraft at high angles of attack was reported.[2]

However, the first truely successful application followed in the 1990s with flaps on an airfoil in a wind tunnel. These experiments of Müller and Patone[3] could demonstrate the beneficial effect of free-movable flaps for low Reynolds numbers ($Re < 150.000$). Bechert et. al.[4] extended the investitations to a typical glider Reynolds number of $Re = 10^6$. The desirable behaviour of self-activated flaps at different angles of attack is shown in fig. 2. At low incidence, the flap remains attached to the airfoil surface and does not have any effect on the aerodynamics. However, with increasing angle of attack when flow separation in the trailing edge region occurs, the flap lifts and self-adjusts to a position dependant on the aerodynamic forces and flap weight.

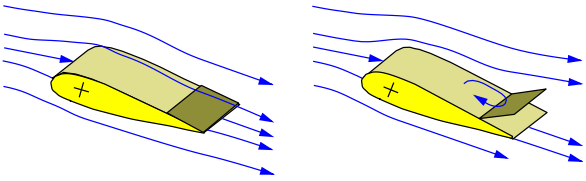

Fig. 2 The self-adjusting flap is closed at low angle of attack and pops up automatically at higher angles.

Self-activated flaps are a tool of passive flow control, meaning that no external energy required by the control mechanism. The opening and closing mechanism is activated by the mean flow itself. Compared to active flow control devices such as periodic suction and blowing or driven flap oscillations, the present approach forms a simple and cost-effective tool that promises to improve the performance of technical high-lift devices.

The goal of the present investigation is to provide a detailed description of the relevant flow physics for self-adjusting movable flaps on airfoils. At first, initial wind tunnel experiments were performed in order to obtain an overview of the general behaviour and to set a proper flap design for the following more detailed experimental and numerical investigations. Finally, movable flaps were installed on a glider plane for free-flight testing.

Experimental Investigation

An initial experimental investigation forming part of a previous study[4] has been carried out with a real glider wing section in a wind tunnel. Lift and drag were measured using a balance. The Reynolds number was between $Re = 1{-}2{\cdot}10^6$, such that the lower flight velocities of the real aircraft were covered. This particular regime is relevant for the high-lift condition under consideration. All investigations have been performed in the low-speed wind tunnel of the Hermann-Föttinger-Institute for Fluid Mechanics at the Technical University Berlin.

Movable flaps on wings: artificial bird feathers

In initial wind tunnel trials, it emerged that the naïve approach of emulating bird feathers by simply attaching multiple plastic strips to the wing surface produced rather confusing results. Therefore, the experiments were continued with a simpler device, i.e., a thin movable flap on the upper surface of a glider airfoil. The flaps used consisted either of flexible plastic material or thin sheet metal. The flaps were attached in the rear part of the airfoil and could pivot on their leading edges (Fig. 3).

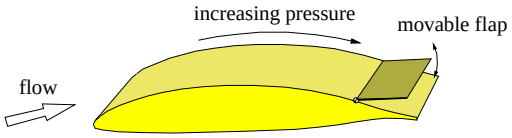

Fig. 3 HQ17 wing section with movable flap.

Under attached flow conditions, the movable flap is very slightly raised. This is due to the fact that the static pressure increases in the downstream direction in the rear part of the upper surface of the airfoil. Thus, the space under the flap is connected to a regime of slightly elevated static pressure. Consequently, in most places, the pressure beneath the movable flap is higher than above it. This behaviour turns out to be not at all advantageous. The drag is slightly increased due to the small separation regime at the end of the flap. In addition, there is a slight decrease in lift, because the angle of the airfoil skeleton line at the trailing edge is decreased and the effective angle of attack of the

airfoil is also decreased. So far, therefore, the impact of the movable flap is a slightly detrimental one. However, there are several ways to deal with this problem. The first and most obvious possibility would be to lock the movable flap onto the airfoil surface under attached flow conditions. The second is also rather simple: The flap could be made porous in order to obtain equal static pressure on both sides of the flap under attached flow conditions. A third method is to make the trailing edge of the flap jagged, as can be seen in fig. 4. This also gives rise to an exchange of pressures. Incidentally, the latter two modifications are in fact characteristic of bird wings.

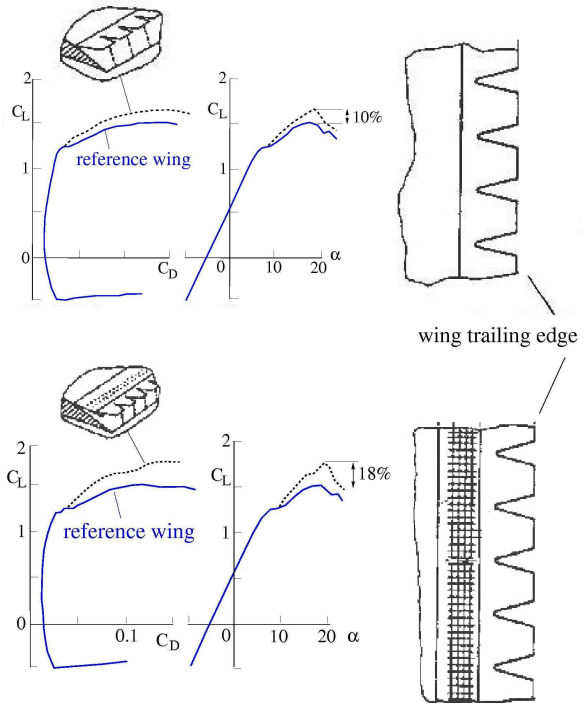

Fig. 4 Data of different variants of movable flaps installed on a laminar glider airfoil.

Now, how do the movable flaps respond to reversed flow? First, it should be mentioned that the velocities in the reversed flow region are considerably smaller than the mean flow velocity. Thus, the movable flaps must be very light and should respond with high sensitivity to even weak reversed flows. A very soft trailing edge of the movable flaps facilitates such a sensitive response. Again, this feature is evident with bird feathers. Once the flow starts to separate, the movable flap follows gradually. It does not, however, protrude into the high speed flow above the separation wake. This high speed flow would push the flap back to a lower elevation. It is useful to stress the marked difference between the movable flaps and a conventional rigid spoiler on a wing:[5] A spoiler protrudes into the high-speed flow regime and increases the width of the wake. In this way, it increases the drag and reduces the lift. By contrast, at high angles of attack, the moveable flap has the opposite effect, i.e. reducing drag and increasing lift. At the same time, the effective shape of the airfoil changes due to the slightly elevated flap and a lower effective angle of attack ensues. Thus, the pressure distribution on the airfoil is adjusted in such a way that the tendency for flow separation is reduced. Consequently, the flow remains attached up to higher angles of attack and the lift of the wing is increased.

Nevertheless, there are limits for everything. At very high angles of attack, the reversed flow would cause the flap to tip forwards entirely and the effect of the flap would vanish. That, however, can be prevented by limiting the opening angle of the flap. Very simply, this is achieved by attaching limiting strings to the movable flap. The optimal maximum opening angle of the flaps was determined experimentally. It was found to lie between 60° (for solid and porous flaps) and about 90° (for flaps with jagged trailing edges). Once the full opening angle is reached, the separation jumps forward over the flap. Hence, for very high angles of attack, the effect of the movable flap finally decreases and vanishes. On birds, tipping over of the feathers is not observed. The feather shafts are sufficiently stiff and well anchored to prevent this detrimental occurrence.

Parameters for flap design optimization

An important question concerns the location on the airfoil where a movable flap should be installed. The experiments started with movable flaps located at the downstream end of the airfoil. This appeared reasonable, because on laminar airfoils, the first 60- 70% of the upper surface is designed to remain laminar. Any attachment or other deviation from a perfectly smooth surface in this laminar regime would cause transition, entailing significant additional drag. On bird wings which operate at lower Reynolds numbers, however, surface smoothness is less important. By contrast, on the rear part of the airfoil and downstream of the laminar regime, minor changes in the surface quality do not produce a detectable increase of the drag. It was found in the experiments that the trailing edge of the movable flap should be located slightly upstream ($\geq$ 1% chord) of the trailing edge of the airfoil, otherwise it would not respond properly to flow separation. On the other hand, the farther upstream the flap is located, the farther upstream the flow separation would have to have already spread before the flap starts to respond. Thus, if influence of incipient separation is desired, the trailing edge of the flap should be located close to the trailing edge of the airfoil.

Another intriguing question involves the size of

a movable flap. The wind tunnel experiments started with comparatively small flaps having a length of about 12% of the airfoil chord length. The effect was significant (Fig. 4) and resulted in an increase of maximum lift of 10%. Increasing the flap length produced a further increase of maximum lift. For instance, a flap length of 22% resulted in an increase of 18% of the maximum lift. However, for large movable flaps (which are not flexible), the self-adjustment to the flow situation becomes less satisfactory. Typically, a movable flap starts to raise when the flow separation has already reached its upstream edge. On the other hand, full reattachment of the flap is obtained at that lowered angle of attack when the reattachment line of a reference wing (without movable flap) has moved downstream to the location of the flap trailing edge. That creates a significantly different behaviour for increasing angles as compared with decreasing angles. This hysteresis in the airfoil data is not desired because it would make an aircraft difficult to handle. One way to avoid this problem is to divide the flap into movable parts attached to each other. Indeed, this double flap adjusts itself much better and the hysteresis is practically eliminated. Nevertheless, the impressive increase in maximum lift is still maintained.

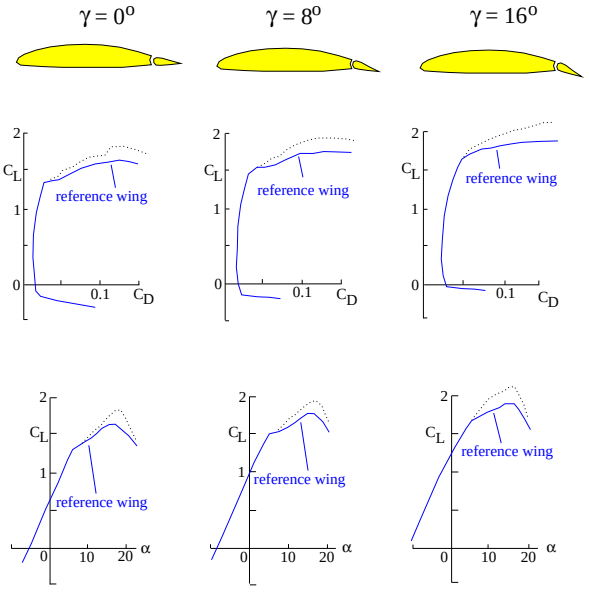

Fig. 5 Combination of conventional and movable flaps for three different flap angles γ. Dotted curves: with movable flap.

From these fundamental investigations, an optimum flap configuration exhibiting high reliability and freedom from hysteresis was identified. The configuration airfoil is a HQ17 of Horstmann und Quast[6] at a Reynolds number of $Re = 10^6$ and a wide range of incidence. The flap is mounted on the airfoil at $x/c = 0.8$ via a free-moving hinge. The maximum flap angle is however constrained to 57°. The main body of the flap is constructed from an aluminium sheet, with the trailing edge made of flexible plastic film.
This configuration forms the base of the current, more detailed experimental and numerical investigations. In the experimental work, pressure distributions as well as separation positions and transition locations are to be measured. A description of the numerical simulations now follows.

Numerical Method

The applied numerical code ELAN, of the Technical University Berlin, is based on a three-dimensional incompressible Finite-Volume scheme to solve the Navier-Stokes equations. The method is fully implicit and of second order in space and time. Based on the SIMPLE pressure correction algorithm, a co-located storage arrangement for all quantities is applied. Convective fluxes are approximated by a TVD-MUSCL-scheme.

Turbulence modeling

The simulation program can be run in an *URANS* mode, solving the *Unsteady Reynolds-averaged Navier-Stokes equations* using statistical turbulence models as well as in a mode for *Large-Eddy Simulation (LES)* or combinations of both.
In simulations of unsteady turbulent flows by Reynolds-averaged approaches, the treatment of turbulent time-scales always requires special attention. An important assumption in the derivation of statistical turbulence models is that time-averaging can be used instead of ensemble-averaging. Therefore the applicability of these models depends on the existence of a *spectral gap* of one or two orders between the resolved time-scales and the modelled scales. Otherwise a formal conflict can arise from an overlapping of resolved and modelled motions. The turbulence model will transfer engergy from the large-scale motion into dissipation, but a URANS approach cannot provide a counteracting mechanism (*back-scatter*). As the occuring turbulent time-scales are not known in advance, the entire flow field needs to be checked for the smallest occuring turbulent time-scales. The resolved time-scales of the large-scale motions have to be significantly larger than the high-frequency small-scale motions that are captured by the turbulence model. Problems can occur if parts of the spectrum are modelled as well as resolved.
In previous URANS investigations with a large variety of different one- and two-equation turbulence models as well as Explicit Algebraic Reynolds-stress Models (EARSM) the LLR k-ω model by Rung[7] exhibited the best overall performance for the present case.[8] It is an improved two-equation eddy-viscosity model with special respect to the realizability conditions.

Additionally, hybrid URANS/LES simulations are performed which are also based on Rung's LLR k-ω model. In the transport equation for the turbulent kinetic energy k, the destruction term is replaced by a formulation based on the turbulent length-scale L_t:

$$\frac{D\varrho k}{Dt} - \mathrm{Diff}(\varrho k) = \varrho \mathrm{Prod}(k) - \beta_k \varrho \underbrace{\frac{k^{3/2}}{L_t}}_{\mathrm{Diss}(k)} \qquad (1)$$

This turbulent length-scale is used to switch between the *URANS* and the *LES* mode, similar to the concept of *Detached-Eddy Simulation (DES)*:[9]

$$\begin{aligned} L_t &= \min\left(L_{t,URANS}, L_{t,LES}\right) \\ &= \min\left(\frac{\sqrt{k}}{c_\mu \omega}, C_{DES}\Delta\right) \end{aligned} \qquad (2)$$

with the specific dissipation $\omega = k/\varepsilon$ and c_μ is the anisotropy parameter in the LLR model and is not constant. In the LES mode, the length-scale $L_{t,LES}$ is given by the definition of Strelets[10] with the constant $C_{DES} = 0.78$ and using the local resolution of the mesh: $\Delta = \max(\Delta x, \Delta y, \Delta z)$.
Most of the numerical simulations are based on the Reynolds-averaged approach. One goal is to verify the applicability of statistical turbulence models for this kind of flow and to prove that all important flow features can be captured by a comparison to the results of the hybrid URANS/LES approach.

Transition

The investigated HQ17 airfoil is a laminar airfoil. As laminar flow stretches over large parts of the airfoil, a proper prediction of transition plays an important role for a suitable computational representation of the flow. Therefore transition is fixed by Krumbein's iterative procedure based on the detection of laminar separation.[11]
For the clean airfoil case, transition positions on the suction side have been measured by flow visualization with a mixture of oil and titanium dioxide. Comparison of measured and predicted transition locations indicate that this procedure can be successfully applied to this kind of flow (Fig. 6). In the laminar region the source terms in the turbulence model are switched off and the free-flow conditions are transported until the transition position.

Computational mesh

The computational c-type mesh provides 202 chordwise cells around the main airfoil and 196 around the flap resulting in 37,000 cells in total for the 2d case. In the three-dimensional simulation the mesh consists of 30 layers in the z-direction covering a span of $b = 0.18c$ and has

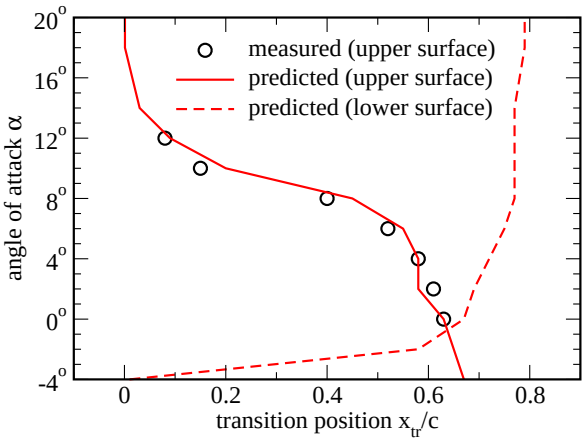

Fig. 6 Measured and predicted transition location for the clean HQ17 laminar profile at $Re = 10^6$.

about 1,000,000 knodes. The non-dimensional wall-distance of the first cell center remains below $Y^+ = 1$ on the complete surface for an attached steady case (Fig. 7). The mesh can represent the clean HQ17 airfoil if the dashed line forms a block interface or a configuration with a flap if the dashed line is modelled as a solid wall. The computational domain covers 6 chords upstream and 10 chords downstream of the configuration. Additional simulations use a 137,000 cells mesh to evaluate the measure of mesh dependency in the 2d case and another mesh covering one chord length in the spanwise direction ($b = c$) in the 3d case.

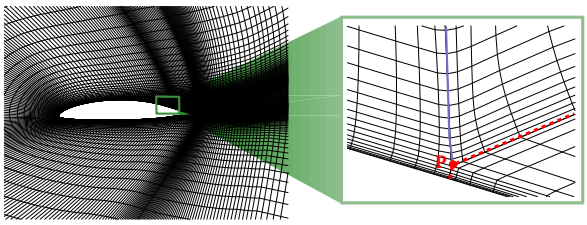

Fig. 7 Computational mesh that represents the clean HQ17 airfoil as well as a configuration of airfoil and flap.

Flap motion

The flap is modeled as a solid body and has only one degree of freedom, the flap deflection angle β. The flap motion is then governed by a balance of moments around the hinge center S (Fig. 8).

$$\theta_S \cdot \frac{d^2\beta}{dt^2} = -M_F(t) - M_G(t)\ . \qquad (3)$$

θ_S is the moment of inertia, $M_G(t)$ is a moment caused by the flap weight and $M_F(t)$ is a moment caused by the fluid forces on the flap. Both moments can be represented by non-dimensional coefficients c_G and c_F. $M_F(t)$ is mainly given by the difference between the static pressure at the

upper flap surface (p_u in fig. 8) and the lower flap surface (p_l):

$$c_F = \frac{M_F}{\frac{1}{2}\ \varrho\ c\ u_0^2\ c\ b} = 2 \int_{r=0}^{l_F} \frac{r(p_u - p_l)}{\varrho c^2 u_0^2}\ dr\ , \qquad (4)$$

Equation (3) can be discretized by a second order finite-difference approach and is solved numerically in a loose coupled system together with the flow field.

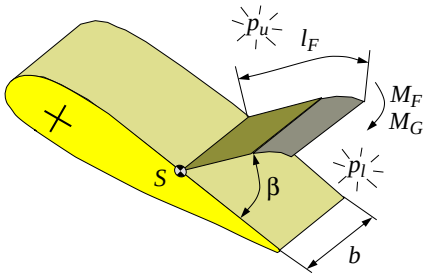

Fig. 8 Sketch of the computational model for the motion of self-adjusting flaps

To capture the geometry in the case of a moving flap, the numerical grid needs to be distortable. Starting with a basic mesh at low flap angle the mesh around the upwards-deflecting flap is deformed using Wick's method based on an analogy to structural mechanics[12] for each time-step. If neccessary, a biharmonic smoothing algorithm is applied to improve the mesh quality.

Numerical Results

The investigations cover two- and three-dimensional simulations of static flaps as well as two-dimensional simulations of free-movable flaps. From initial numerical investigations of the clean airfoil, it was known that the flow becomes unsteady at high angles of attack and vortex shedding occurs. Therefore all computations are unsteady with a typical time-step of $\Delta t = 0.01 c/u_0$. For detailed information about the flow around the HQ17 reference profile see Schatz.[8]

Static flap

The first step of modeling free-movable flaps is to run a series of simulations with a static flap at different deflection angles and angles of attack. The analysis of these compuations allows the identification of one flap position for each angle of attack where the flap moment M_F and the gravity moment M_G are balanced ($c_F = -c_G$). This equilibrium position should correspond to the mean location of a self-adjusting flap.
In fig. 9 the resulting flap coefficient c_F is plotted for different flap angles and incidences. Positive quantities mean that the flap is pushed downwards

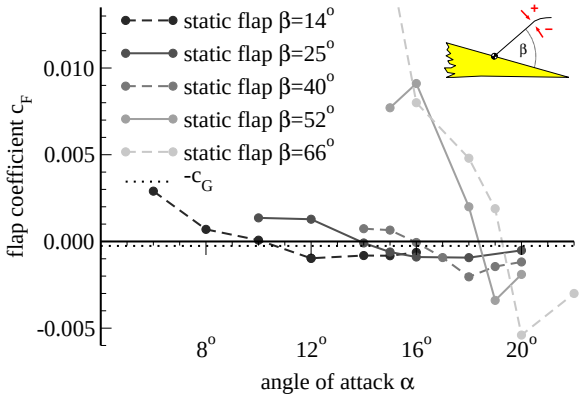

Fig. 9 Flap coefficient c_F for varying deflection angle β.

by the fluid and in the case of negative c_F it will pop up.
For further analysis, isosurfaces of the mean flow velocity in x-direction are plotted in fig. 10. The edge of the reverse flow region ($u = 0$) is marked by a black line. It is found that an optimum angle β is achieved when the flap just slightly touches the detached shear-layer. In the case of lower flap angles, the flap remains inside the reverse flow region which it splits into two parts. On the mean lift, however, it shows less effect (right column in fig. 10). In the case of excessive angles the flap works like a spoiler and generates additional drag (left column in fig. 10).

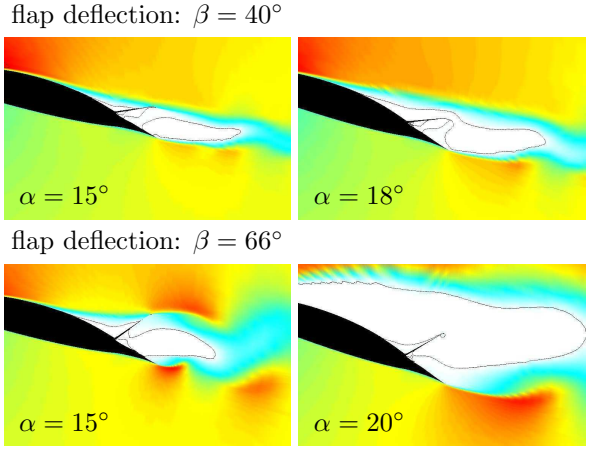

Fig. 10 Mean flow velocity in x-direction, rows have different flap deflection β and columns with different angle of attack. left: excessive flap deflection, right: insufficient flap deflection.

The unsteady flow in the wake can be stabilized by flaps at low flap angles and at the same time the size of detaching vorticies as well as the amplitude of lift oscillations decrease. This effect is comparable to that of a splitter plate[13] in the wake of cylinders.
For each flap deflection angle β, a lift polar with

the typical shape is computed. With increasing flap deflection the camber ratio of the configuration decreases and the polar is shifted to the right (this behaviour makes spoilers a very effective tool for the destruction of lift). As each of these polars exceeds the reference wing in a particular region of incidence, higher lift coefficients are shown to be possible (Fig. 11). The envelope curve of all polars, representing the maximum achievable lift by static flaps, promises a gain in lift of up to 18%. In the equilibrium position, however, the lift remains below this maximum and only a gain of about 15% can be observed (Fig. 17). These results match almost perfectly with the experimental wind tunnel results.

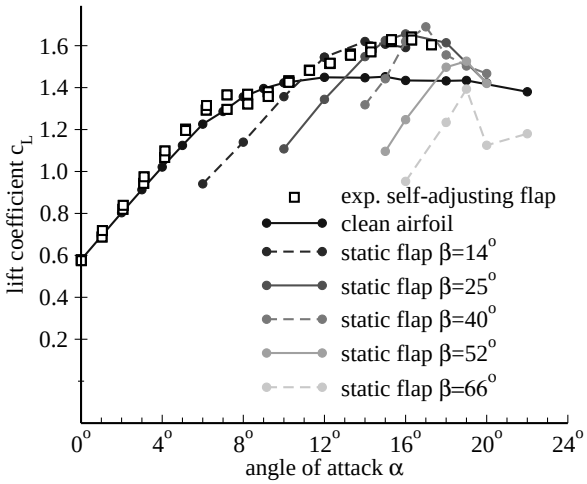

Fig. 11 Lift coefficient for the HQ17 airfoil with static flap at different deflection angle β.

At the same time the flow detachment from the airfoil upper surface can be delayed by the flap. Fig. 12 shows that between $\alpha = 10°$ and $\alpha = 20°$, the flow is able to remain attached longer than in the reference airfoil case. Here the numerical simulations exhibit the same quantitative effect of the flap like the experiments, where flow separation is detected by flow visualization with a mixture of oil and titanium dioxide. However, a constant shift between the experimental and numerical results occur.

For the next step the numerical investigations are extended to the three-dimensional case. First the clean airfoil is simulated and, following this, an airfoil with a flap that covers the complete span. The three dimensional simulations indicate that the flow remains two-dimensional as long as the geometry is two-dimensional. Contour plots of mean flow quantities (e.g. the vertical velocity component in fig. 13) show almost no three dimensionality.

Finally, a flap extending over only part of the wing span is computed. For low angle of attack and large flap deflection, the effect is comparable to

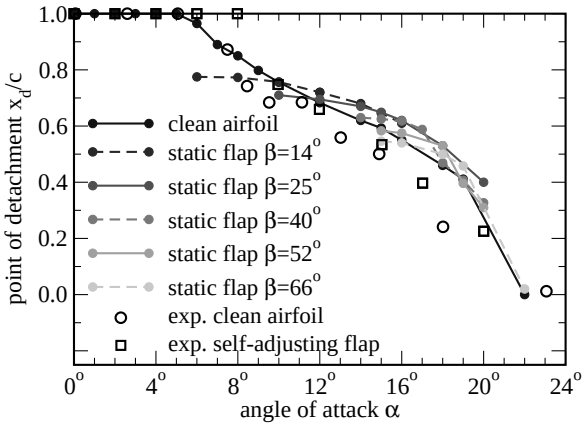

Fig. 12 Point of flow detachment for the HQ17 airfoil with static flap and ranging deflection.

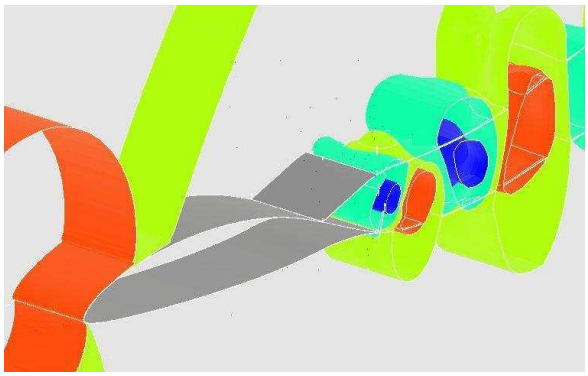

Fig. 13 Isosurfaces of the vertical velocity component for the flow around an airfoil with a static deflected flap ($\alpha = 16°$, $\beta = 40°$).

a spoiler flap and causes strong pertubations in the flow, in particular two vortices at the edges of the flap. The lift of the wing can be completely destroyed by the flap (Fig. 14).

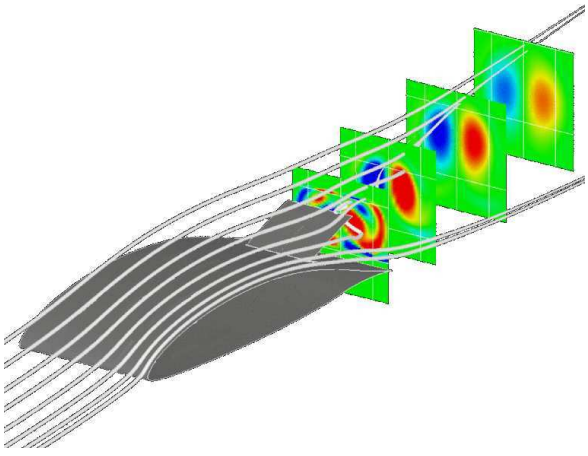

Fig. 14 Streamlines of the flowfield around a static flap at high flap deflection angle ($\beta = 40°$) at an airfoil at low angle of attack ($\alpha = 4°$).

In the case of a flap in an equilibrium position, however, the effect of the flap edges on the flow is

minor. As the boundary layer on the flap surface and the free shear-layer in the spanwise location without flap are very similar, almost no interaction of the flapped and the clean part of the wing can be observed. In this case no significant effect of the flap edge on the opening mechanism of the flap is apparent because almost no fluid forces are acting on the flap ($c_F < 10^{-3}$). Separation is delayed, the lift can be enhanced by the flap and all aerodynamic forces are comparable to the infinite flap case. Fig. 16 gives an impression of the flow around a flap covering part of the wing span.

Hybrid URANS/LES computations

In simulations of unsteady turbulent flows by Reynolds-averaged approaches (URANS), turbulent time-scales always require special attention. The resolved time-scales of the large-scale motions have to be significantly larger than the high-frequency small-scale motions that are captured by the turbulence model. Problems can occur if parts of the spectrum are modelled as well as resolved. In the present investigations, the entire flow field is checked for the smallest occuring time-scales. Particularly in the near wake behind the airfoil, the turbulent frequencies cover the same range of the spectrum as the resolved time-scales. Consequently, the application of the Reynolds-averaged approach is questionable. It should also be remarked that the turbulent frequencies depend on the time-stepping itself. In order to prove the reliability of the simulation, additional investigations with a hybrid URANS/LES method are performed which should avoid the time-scale problem.

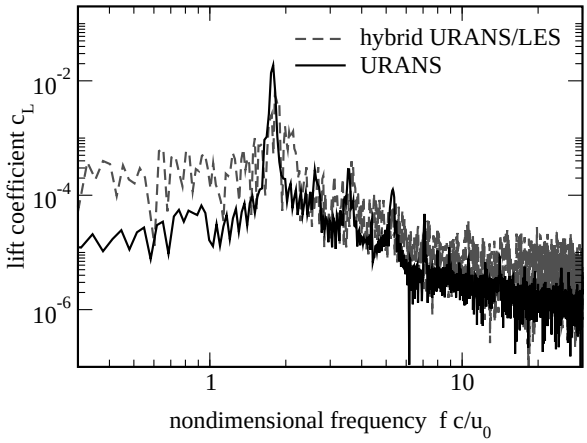

Fig. 15 Frequency spectrum of lift for URANS and the hybrid URANS/LES method for the flow around an airfoil with static flap.

Hybrid URANS/LES results obtained on the same numerical mesh with the same time-step can be compared to the URANS computations. Both methods give similar mean aerodynamic forces. The unsteady features of the flow can be compared by a spectrum of lift in fig. 15. One dominant peak coresponding to the same shedding frequency can be indentified in the results of both methods. However, the level of "noise" in the Hybrid URANS/LES simulation is much higher than in the Reynolds-averaged method. In fig. 16, iso-surfaces of the w-velocity and contours of eddy-viscosity for the hybrid approach results of the case of a wing with a $b/c = 10\%$ flap are presented for $\alpha = 16°$ angle of attack. The flowfield does not show significant differences in the time-averaged quantities compared to URANS.

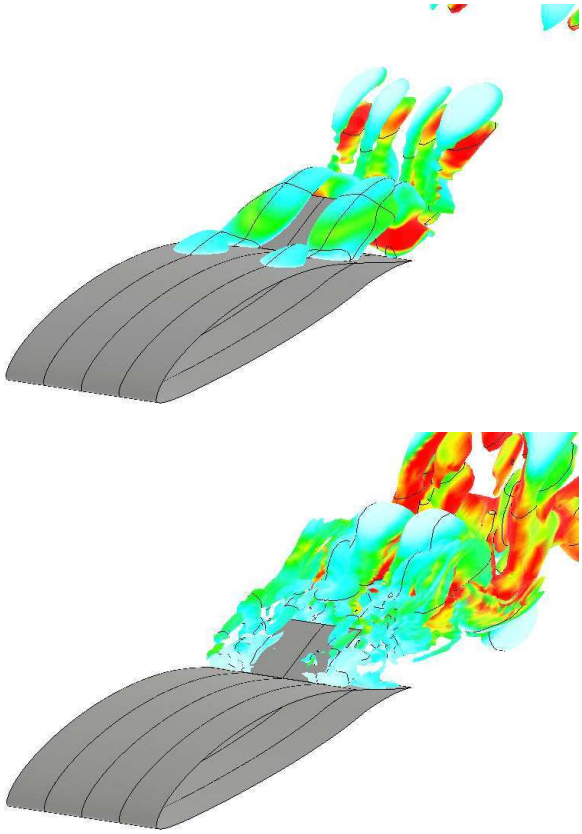

Fig. 16 Iso-surfaces of the spanwise velocity colored by contours of turbulent viscosity of the hybrid URANS/LES approach, flow around static flap. Upper figure: URANS results (dark corresponds to $\nu_t = 1000\nu$), lower figure: results of hybrid approach (dark corresponds to $\nu_t = 200\nu$).

Freely movable flap

In the present investigations the flap motion is modelled by a coupled fluid-structure interaction method. It was seen that the flap finds this equilibrium position by itself, and furthermore, this position is stable. The lift coefficient is augmented by the deployment of the flap and can be increased by 12.9% compared to the clean airfoil (Fig. 17). At high angles of attack, the flowfield is dominated by flow separation. In the range of incidence when the self-adjusting flap is active, the detachment can

be significantly delayed (Fig. 18). These numerical results are in good agreement with the experimental data.

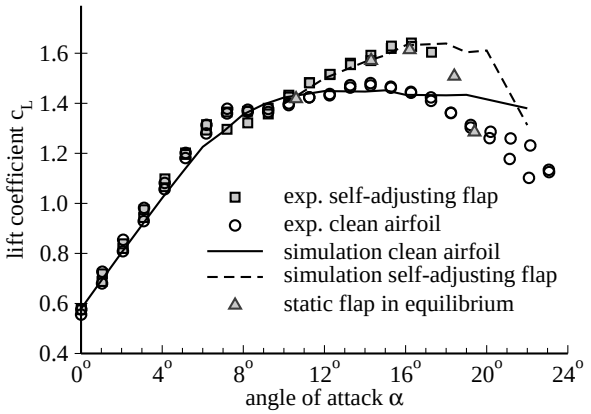

Fig. 17 Lift coefficient for the HQ17 airfoil with self-adjusting flap.

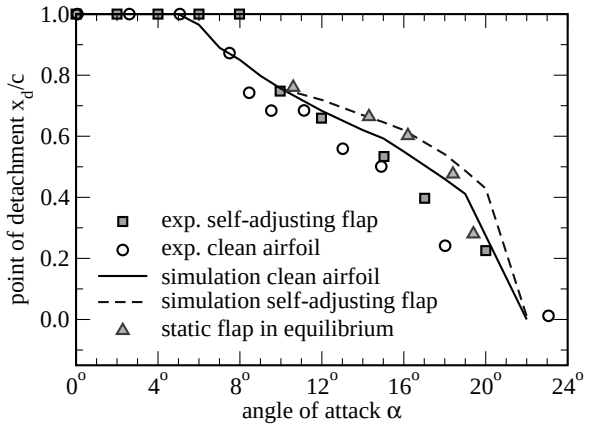

Fig. 18 Point of flow detachment for the HQ17 airfoil with self-adjusting flap.

In the URANS computations, the flowfield in the wake is dominated by a single fluctuation frequency. Based on the flap length, it corresponds to a nondimensional Strouhal number which is plotted in fig. 19. The Strouhal number for the self-adjusting flap is slightly higher compared to that of the clean airfoil, but no difference to the static flap is visible.

The flap also has a stabilising effect on the turbulent wake. The mean deflection angle differs from the equilibrium position of the static flap, and as fig. 20 shows, it is slightly lower than that observed in the experiments. Due to the relatively crude modeling of the flap-tip shape, all deflection angles are slighly underpredicted in the compuations.

The numerical simulation provides the possibility of quantification of the intensity of the backflow in the reverse flow region. The nondimensional reverse flow factor c_R is defined by:

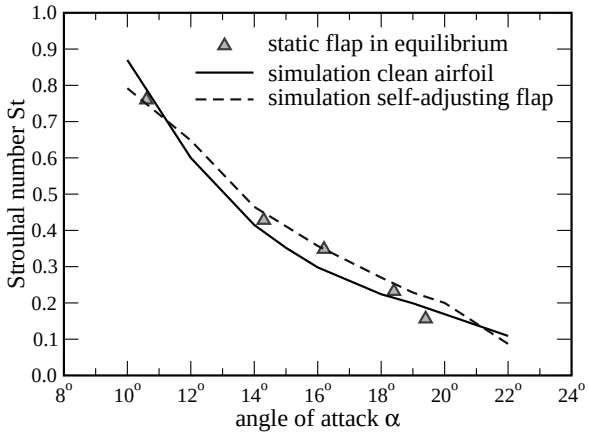

Fig. 19 Strouhal number for different angles of attack.

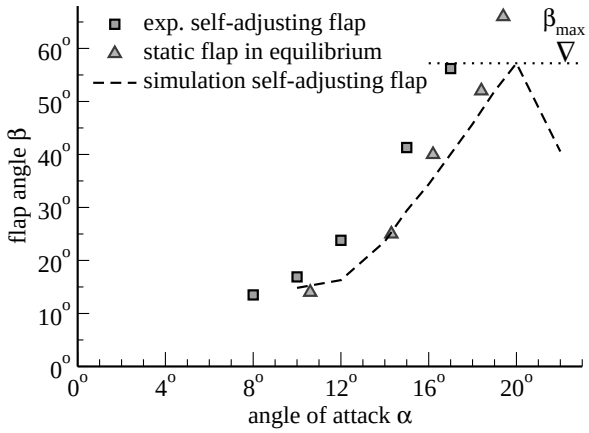

Fig. 20 Deflection of a self-adjusting flap in comparison to a static flap in equilibrium position and to experiments.

$$c_R = \frac{\dot{m}_R}{\dot{m}_0} = \frac{1}{\varrho c^2 u_0} \int_{y=0}^{y(u=0)} \varrho u_i \, dA_i \, . \qquad (5)$$

This factor is computed for the clean airfoil and the airfoil with a self-adjusting flap. Fig. 21 shows that over a wide range of incidence, the reverse mass-flow can be significantly reduced by the flap. One important effect is based on the division of the separated flow region into two parts, with much lower intensity than in the clean airfoil case.

Comparison of experiments and numerical simulations in the predicted pressure distribution at $\alpha = 18°$ angle of attack are shown in fig. 22. In both experiment and numerical simulation, a shift in the pressure between the upper and the lower surface of the flap is clearly visible. As a consequence, the flow on the upper surface is able to remain attached for a longer range of chord. Part of the lift is generated by slightly higher pressure on the lower surface which can be observed in both figures.

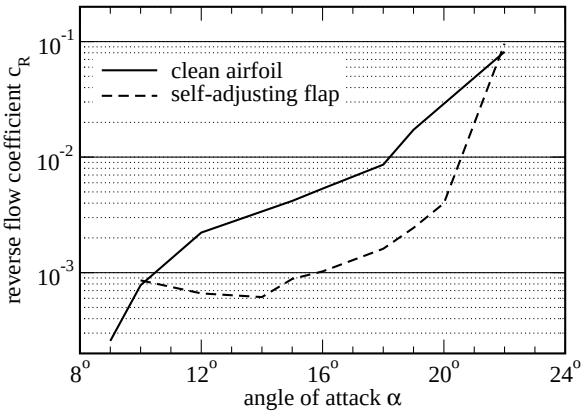

Fig. 21 Reverse flow coefficient c_R at $x/c = 0.99$ for the self-adjusting flap compared to the clean reference airfoil.

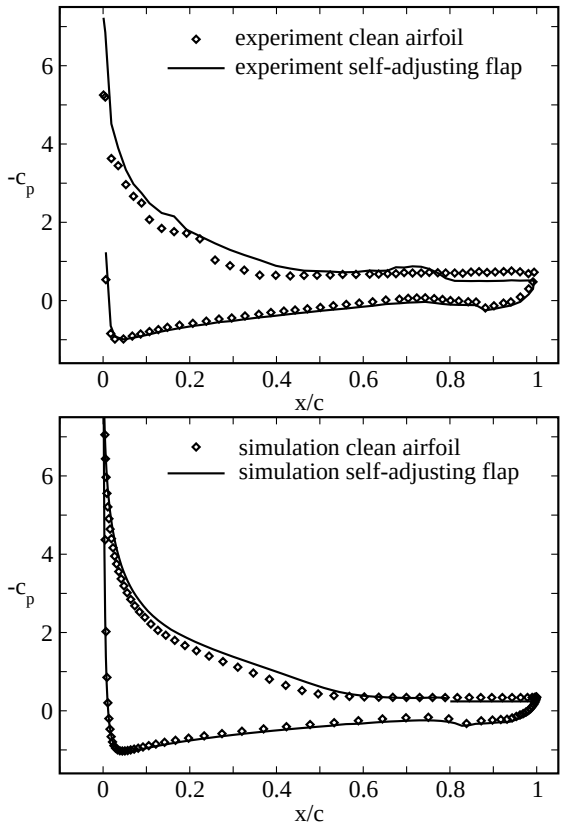

Fig. 22 Pressure distribution on the airfoil at $\alpha = 18^\circ$ with and without movable flap. Upper figure: experimental results, lower figure: computational results.

For swept wings, the occuring cross-flow interacts with the reverse flow responsible for the opening of the flap. Consequently, self-adjusting flaps are not able to provide satisfactory performance on swept wings.[14]

Influence of flap-mass

The equilibrium position, however, does not provide the maximum achivable lift. Lower flap angles result in higher efficiency. Flaps with increased mass move to a lower flap deflection due to the higher gravity. This small β has a benefitial effect on the mean lift which can be enhanced by 15.3% as opposed to 12.9% from a tripled mass flap (Fig. 23). Unfortunately, in the experiments it became clear that excessively heavy flaps inhibit the automatic opening mechanism.

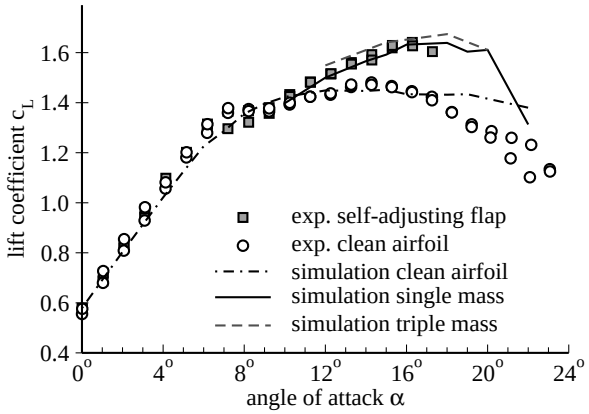

Fig. 23 Lift coefficient of an airfoil with free-movable flaps of different mass.

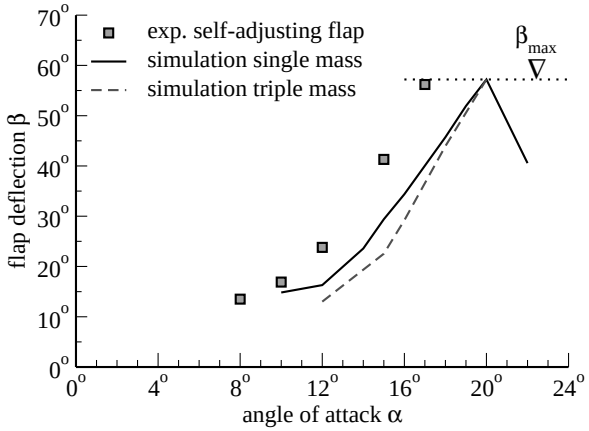

Fig. 24 Mean flap deflection β of free-movable flaps with varying mass.

Flight Experiments with Movable Flaps

After wind tunnel testing and theoretical analysis, self-adjusting flaps have been installed on an aircraft for free flight tests. The aircraft available for the this experiments was a STEMME S10 motor glider. Using its piston engine, it can take off unassisted and the foldable propeller can be retracted into the nose of the cockpit. During flight, the motor can be re-started if necessary. With retracted propeller, the aircraft is a fast high-performance glider. The laminar wing is equipped with conventional flaps which also function as ailerons. The HQ41 airfoil cross-section deviates only minimally from the HQ17 (Fig. 3) whose coordinates are given in a description of the

experiments.[4] As a specific preparation for flight experiments with this aircraft, it was assured that the movable flaps would also work properly in combination with the conventional flaps on the wings. Fig. 5 shows data with both types of flaps combined. The movable flap is actually mounted on the conventional flap. As can be seen, the increase of lift caused by the movable flap is reproduced. During the flight experiments, the intention was to fly at very high angles of attack encroaching on the regime of total stall. Usually, for tests of high-lift systems, one does not go so far in order to avoid dangerous situations such as spinning of the aircraft. These flight tests, however, included such situations with the purpose of demonstrating the inherent safety of the movable flaps. This required:

(i) a very skilled pilot, well familiar with the behaviour of the aircraft,

(ii) sufficient altitude during critical flight phases to have sufficient time available for the pilot to handle the arising situations, or in the worst case, (which did not occur) to bail out,

(iii) the introduction of the attitude changes in a gradual stepwise fashion in order to avoid unfamiliar situations for the pilot,

(iv) a "special preparation" of the aircraft to keep it controllable.

The latter "special preparation" can be seen in fig. 25. The elevator was equipped with vortex generators on the upper surface in order to extend its angular regime of attached flow. The same vortex generators were installed on the outer parts of the wings. This caused an increase of maximum lift of 31%. However, some peculiar flight-dynamical effects were caused by this: the return to normal flight attitude from the stall-spinning sequence sometimes resulted in spin in the opposite direction. This was probably caused by the exaggerated asymmetry in lift between attached and fully separated flow conditions on the outer wing, due to the vortex generators.
A reduction to half the previous number of the vortex generators (i.e., a reduced V.G. density) reduced the increase of maximum lift to merely 15% on the outer wings. This turned out to be more compatible with the original flight-dynamical layout of the aircraft and thereby eliminated the problem. In addition, the performance of the outboard wing section then became closer to the inboard section with movable flaps. Incidentally, for the solution of these safety-relevant problems it proved very useful to that the full-scale wind tunnel experiment was available in parallel to the flight tests. In order to highlight the flow situation on the wing, woolen tufts were attached to its surface. These

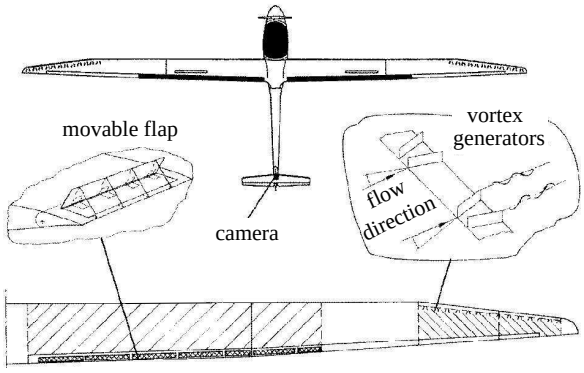

Fig. 25 STEMME S10 test aircraft, equipped with movable flaps and vortex generators.

and the motion of the movable flaps were recorded by a video camera on the empennage. On the video tape the flight speed was also recorded. Typical flow situations can be seen in fig. 26. The video pictures in fig. 26 are fully consistent with parallel experiments in the wind tunnel at identical air speed and Reynolds number. In flight experiments, the increase in maximum lift coefficient c_L can be documented by recording the minimum attainable speed before stall. Therefore, during the tests, the flight speed had been reduced very gradually until total stall occurred. The reduction in minimum speed due to the movable flaps was recorded in this way. For comparison, test flights were also carried out where the movable flaps had been locked. The reduction in minimum speed due to the movable flaps was 3.5%. That corresponds to a 7% increase of lift. Taking into account that only 61% of the wing area was equipped with movable flaps, one obtains an 11.4% increase of maximum lift for the airfoil. This is almost exactly the same value that had been obtained previously in the wind tunnel and by the numerical simulation with the same movable flap.
The comments of the pilot were also positive. Permanent spinning did not occur following a straight-flight stall situation. By contrast, with locked movable flaps, permanent spinning did develop from the same situation. However, due to our cautiousness, the flaps were only installed in the inner part of the wing. Therefore, the changes in flight behaviour were only moderate, albeit positive. Another observation was that keeping the flight speed at low and near-stall values appeared to be easier with movable flaps. More detailed information can be found in a report on this subject.[15]

Summary

The effect of self-adjusting movable flaps on airfoils similar to the outer layer of feathers on the upper surface of bird wings has been demonstrated in experimental and numerical investigations. It has been shown that lift can be enhanced by more than 10%. The main effect of the flap can be de-

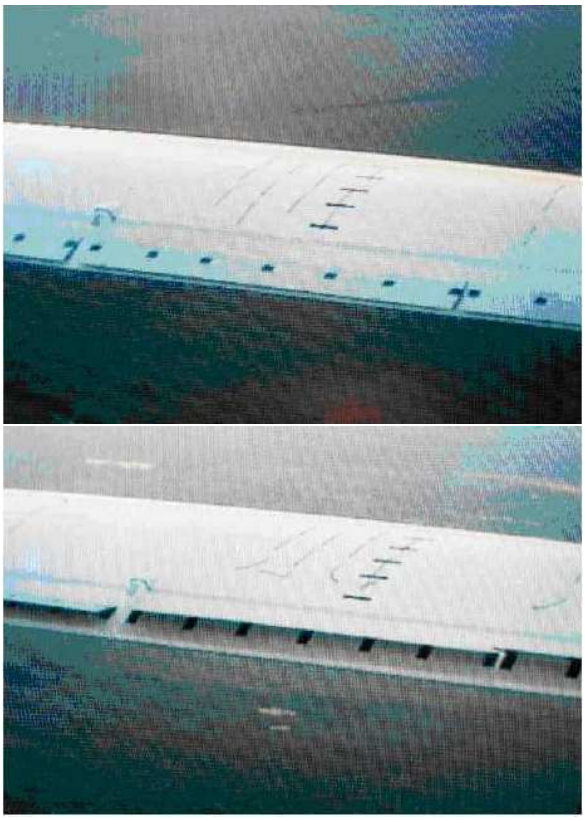

Fig. 26 In-flight video recording. The upper picture shows attached flap and attached flow. On the lower picture, the woolen threads indicate partial separation and the movable flap has raised by itself.

scribed as a blockage of the reverse flow from the trailing edge region to the suction peak resulting in a delayed flow separation.

This simple and cost-effective flow control tool can be combined with other devices. Its performance has already been demonstrated in free-flight experiments with a glider airplane. The application is however limited to subsonic flows and non-swept wing configuration.

Acknowledgement

This research is funded by the German National Science Foundation (DFG) under the umbrella of the Special Research Activity (Sonderforschungsbereich, Sfb 557, 'Beeinflussung komplexer turbulenter Scherströmungen') at the Technical University Berlin. The person who took the highest personal risk in this project was the test pilot P. Montag of the STEMME Aircraft Company, Strausberg. In addition, we appreciate the support by Dr. R. Stemme and M. Lang of this company. A test wing was supplied by A. Quast, DLR Braunschweig. Very valuable comments and advice were provided by Prof. W. Liebe, Berlin and Dr. J. Mertens, DaimlerChrysler Aerospace Airbus GmbH, Bremen. Financial support was supplied by the Volkswagen-Stiftung and the German Federal Ministry of Science, Technology and Education (BMBF) and is gratefully acknowledged.

References

[1]W. Liebe. Der Auftrieb am Tragflügel: Entstehung und Zusammenbruch. *Aerokurier*, 12:1520–1523, 1979.

[2]B. Malzbender. Projekte der FV Aachen, Erfolge im Motor- und Segelflug. *Aerokurier*, 1, 1984.

[3]G. Patone and W. Müller. Aeroflexible Oberflächenklappen als "Rückstrombremsen" nach dem Vorbild der Deckfedern des Vogelflügels. TR-96-05, Technische Universität Berlin, 1996.

[4]D.W. Bechert, M. Bruse, R. Meyer, and W. Hage. Biological surfaces and their technological application – laboratory and flight experiments on drag reduction and separation control. *AIAA Paper 97-1960, Snowmass Village, CO*, 1997.

[5]G.V. Parkinson, G.P. Brown, and T. Jandali. The aerodynamics of two-dimensional airfoils with spoiler. In *V/STOL Aerodynamics, AGARD–CP–143*, pages 14/1–14/10. Elsevier, Amsterdam, 1974.

[6]K.H. Horstmann and A. Quast. Widerstandsverminderung durch Blasturbulatoren. Technical report, DFVLR-FB 81-33, 1981.

[7]T. Rung and F. Thiele. Computational modelling of complex boundary-layer flows. In *9th Int. Symp. on Transport Phenomena in Thermal-Fluid Engineering, Singapore*, 1996.

[8]M. Schatz. *Numerische Simulation der Beeinflussung instationärer Strömungsablösung durch frei bewegliche Rückstromklappen auf Tragflügeln.* PhD thesis, Technische Universität Berlin, Mensch & Buch Verlag, Berlin, 2003.

[9]P.R. Spalart, M. Shur, M. Strelets, and A. Travin. Detached-eddy simulation of an airfoil at high angle of attack. In *Engineering Turbulence Modelling and Experiments – 4*. Elsevier, Amsterdam, 1999.

[10]M. Strelets. Detached-eddy simulation of massively separated flows. *AIAA Paper 2001-0879*, 2001.

[11]A. Krumbein. On modeling of transitional flow and its application on a high lift multi-element airfoil configuration. *AIAA Paper 2003-0724*, 2003.

[12]A. Wick. A novel method for generation of dynamic meshes. In *7th International Conference on Numerical Grid Generation in Computational Field Simulations, Sep. 25-28, Whistler, Canada*, 2000.

[13]E.A. Anderson and A.A. Szewczyk. Effects of a splitter plate on the near wake of a circular cylinder in 2- and 3-dimensional flow configurations. *Experiments in Fluids*, 23:161–174, 1997.

[14]R.K.J. Meyer. *Experimentelle Untersuchungen von Rückstromklappen auf Tragflügeln zur Beeinflussung von Strömungsablösung.* PhD thesis, Technische Universität Berlin, Mensch & Buch Verlag, Berlin, 2000.

[15]R. Meyer, D.W. Bechert, W. Hage, and P. Montag. Aeroflexible Oberflächenklappen als Rückstrombremsen nach dem Vorbild der Deckfedern des Vogelflügels. IB 92517-96/B5, DLR, 1997.

[16]D.W. Bechert, M. Bruse, W. Hage, and R. Meyer. Review article: Fluid mechanics of biological surfaces and their technological application. *Naturwissenschaften, Springer*, 87:157–171, 2000.

[17]P.W. Bearman. Investigation of the flow behind a two-dimensional model with a blunt trailing edge and fitted with splitter plates. *J. Fluid. Mech.*, 21:241–255, 1965.